Generation and detection of guided waves using PZT wafer transducers

J.H. Nieuwenhuis[1,2], J. Neumann,[3] D.W. Greve,[3] and I.J. Oppenheim[4]
[1] Institute of Sensor and Actuator Systems, Vienna University of Technology, Austria
[2] Vienna University of Technology, Vienna, Austria
[3] Department of Electrical and Computer Engineering, Carnegie Mellon University, Pittsburgh, PA, USA
[4] Department of Civil and Environmental Engineering, Carnegie Mellon University, Pittsburgh, PA, USA

Abstract

We report here the use of finite element simulation and experiments to further explore the operation of the wafer transducer. We have separately modeled the emission and detection processes. In particular, we have calculated the wave velocities and the received voltage signals due to A0 and S0 modes at an output transducer as a function of pulse center frequency. These calculations include the effects of finite pulse width, pulse dispersion, and the detailed interaction between the piezoelectric element and the transmitting medium. We show that the received signals for A0 and S0 modes have maxima near the frequencies predicted from the previously published point-force model.

I. Introduction

Many authors have considered the use of Lamb waves for non-destructive testing. Lamb waves can propagate for considerable distances in plates, making it possible to detect flaws over a considerable area with a single transducer. Complications that are encountered include the existence of multiple modes and the dispersive character of the modes. A partial solution to this complexity is the use of transducers that excite only a single mode, and various strategies have been employed in the past in order to achieve this. An angled prism can be used to convert a longitudinal mode into a particular plate mode by appropriate choice of the prism angle [1]. Alternatively, comb-type transducers [1,2,3] or linear arrays with time-delayed excitation [4,5] can be used. There has been recent interest in the use of single PZT wafers as transducers, in part because of the simplicity and potentially low cost of these transducers. Single PZT wafers have been explored with continuous sinusoidal [6,7] or pulsed [8,9] excitation for defect detection in composite panels and the influence of flaws on the Lamb waves has been modeled. In some [6,8] work the use of the A0 mode was recommended, in part because of lower attenuation. Selective excitation of the S0 mode using a PZT wafer bonded to the plate has also been proposed and demonstrated [9]. While a theoretical explanation for the mode selectivity of the PZT wafer transducer has been reported [9], that analysis is strictly applicable only to the sinusoidal steady state and makes numerous simplifying assumptions. In particular, the mechanical interactions between the PZT wafer and the

plate are not included. In addition, this analysis only considered the emission of waves and not the reception, which will will show is physically distinct and that has a different dependence on pulse center frequency.

In this paper, we use a combination of finite element simulation and experiments to further explore the operation of the wafer transducer. We have separately modeled the emission and detection processes. In particular, we have calculated the wave velocities and the received voltage signals due to A0 and S0 modes at an output transducer as a function of pulse center frequency. These calculations include the effects of finite pulse width, pulse dispersion, and the detailed interaction between the piezoelectric element and the transmitting medium. The results obtained provide more accurate predictions of the mode selectivity than have been previously reported using a simplified point-force model [9]. In addition, we are able to determine the optimum PZT wafer thickness. Finally, this approach is readily adapted to explore the interactions of waves with flaws and edge attachments.

In the following section we report simulations of the emission of guided waves using both the point-source and PZT sources. We will show that a simplified model for the PZT wafer provides good accuracy and does not require a full multiphysics simulation. In Section III we simulate the detection of guided waves and combine these results with the emission model to determine the overall transfer function. Section IV compares the simulations with experiment, Section V presents guidelines for transducer design, and Section VI contains overall conclusions.

II. Emission of ultrasonic waves

Figure 1a shows a wafer-type transducer bonded to plate. The plate and wafer are assumed to be of infinite extent in the z direction (this is the plane strain condition in structural mechanics, that is, all strains out of the plane are assumed to be zero). We consider one half of a plate symmetric about the y-axis. The wafer is a piezoelectric material with the poling direction normal to the plate surface and metallized on the top and bottom surfaces. For emission an exciting signal is applied between the metallized surfaces of the plate. In the receive mode the transducer terminals are connected to a high-impedance load such as an oscilloscope.

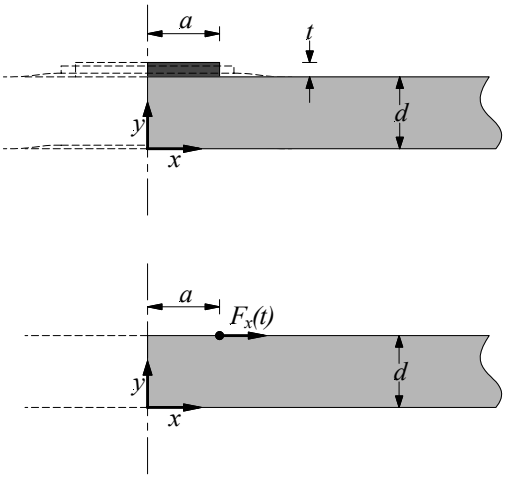

Fig. 1. Geometry for modeling studies: (top) wafer-type transducer bonded to a plate with deformed state indicated in dashed lines; and (b) a point force $F_x(t)$ as used in analytic modeling of the wafer-type transducer.

The figure also illustrates qualitatively the effect of an applied voltage. The PZT is compressively (tensilely) strained in the *y* direction and expands (contracts) in the *x* direction. This results in a traction force on the surface of the plate. There is also a smaller force in the *y* direction on the plate. In the theoretical work by Giurgiutiu [9], it was assumed that the PZT plate exerts a force at a single point in the *x* direction only (Fig. 1b) and the steady-state response of the system was calculated. We have termed this model the point-force model to be consistent with the terminology in the publications of Giurgiutiu. Strictly speaking the force is a line load per unit length in the *z* direction.

In the following, we will simulate the *transient* generation of plate waves in an infinitely wide plate. By using finite element simulation, we can model the PZT wafer and the plate together, and we can calculate the two-dimensional wave that is generated. We will first simulate the effect of a windowed sinusoidal force applied at a single point. These results will be compared with the results of Giurgiutiu [9]. We then simulate the interaction between a PZT wafer and the plate, which more accurately matches the actual physical configuration.

Point source

Figure 1b shows a single point source applied to the upper surface a distance *a* from the *y* axis. The *x* displacement was constrained to be zero at the origin and consequently we model one half of a symmetric domain. All other boundaries were free. Simulations were performed in the time dependent mode with output time steps typically equal to one eighth of a period. Mesh parameters were chosen so that the element sizes were substantially smaller than a wavelength. Some calculations were performed with half the output time step and a smaller element size to verify that these parameters did not have a significant effect on the results. The time-dependent force was given by

$$F(t) = \begin{cases} F_0 \sin(\omega t) \cdot \left(\sin(\frac{\omega t}{10}) \right)^2 & t < \frac{10\pi}{\omega} \\ 0 & otherwise \end{cases} .$$

This yields a smooth windowed sinusoid 5 cycles in length with center frequency ω.

Emission simulations were performed using the time-stepping mode of the two-dimensional plane strain mode of FEMLAB 2.3 (ode23s solver). In all simulations reported below, the plate was aluminum (E = 70 GPa, ρ = 2.7 gm/cm^3, v = 0.33, mass damping coefficient 0, stiffness damping coefficient = 0) 1.59 mm in thickness and the force was applied a distance a = 3.2 mm from the center point. These dimensions were chosen to match the configuration used in experiments described later.

We will report on simulations for frequencies in the range from 33 kHz to 800 kHz. Figure 2 shows the aluminum phase velocity of the A0 and S0 modes as a function of the frequency-thickness product. For an aluminum plate of thickness 1.59 mm, only these two modes exist at frequencies below 1 MHz. According to the simplified analytic model of Giurgiutiu [9], peak emission for a mode i occurs at a frequency $f_{\max}^{i,n}$ where the force baseline is exactly one half of an integral number of wavelengths, that is

$$f_{\max}^{i,n} = \frac{v_{phase} \cdot (n - ½)}{2a} . \quad (1)$$

where n is an integer greater than or equal to one. Similarly, a null in emission occurs at $f_{\min}^{i,n}$ such that the force baseline is an integral number of wavelengths, or

$$f_{\min}^{i,n} = \frac{v_{phase} \cdot n}{2a} . \quad (2)$$

These frequencies can be determined by construction from the phase velocity plot (Fig. 4). For an aluminum plate of 1.59 mm thickness we expect minima $f_{\min}^{A0,1}$ = 283 kHz and $f_{\min}^{S0,1}$ = 816 kHz and maxima $f_{\max}^{A0,1}$ = 86 kHz, $f_{\max}^{A0,2}$ = 517 kHz and $f_{\max}^{S0,1}$ = 419 kHz.

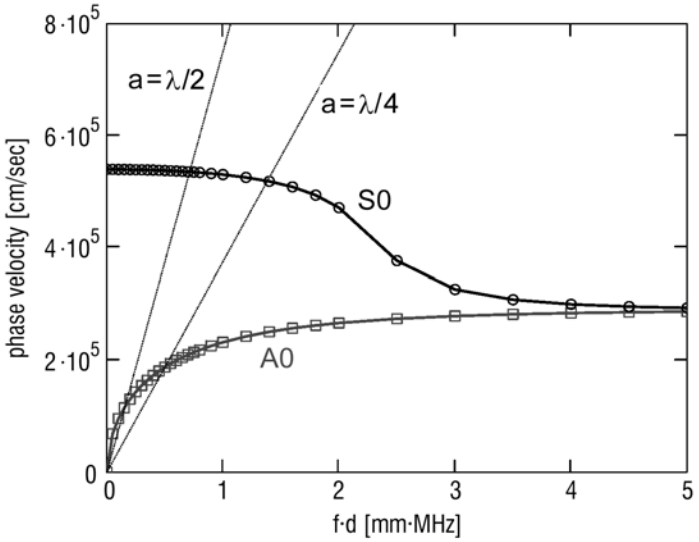

Fig. 2. Calculated phase velocity for A0 and S0 Lamb waves in an aluminum plate as a function of frequency-thickness product. Based on the point-force model maximum emission amplitude is expected when $a = \lambda/2$ and minimum emission amplitude when $a = \lambda/4$.

Figure 3 shows the results for time $t = 4 \times 10^{-5}$ sec from simulations at a range of frequencies. The wave is generated at the left edge and propagates to the right. The colors in this figure indicate the von Mises stress. The arrows indicate the vector particle displacements from the equilibrium position.

The simulations show the expected two propagating modes with S0 and A0 character. The S0 mode has the highest group velocity and shows particle displacements mostly in the x direction, and the slower wave is the A0 mode, which shows particle displacements that are mostly in the y direction and are asymmetric about the center of the plate. Qualitatively, it appears that the relative magnitudes of the A0 and S0 modes vary, with a minimum magnitude for the A0 mode near 300 kHz. This agrees well with the frequency where the wavelength of the A0 mode is equal to the total length of the force baseline.

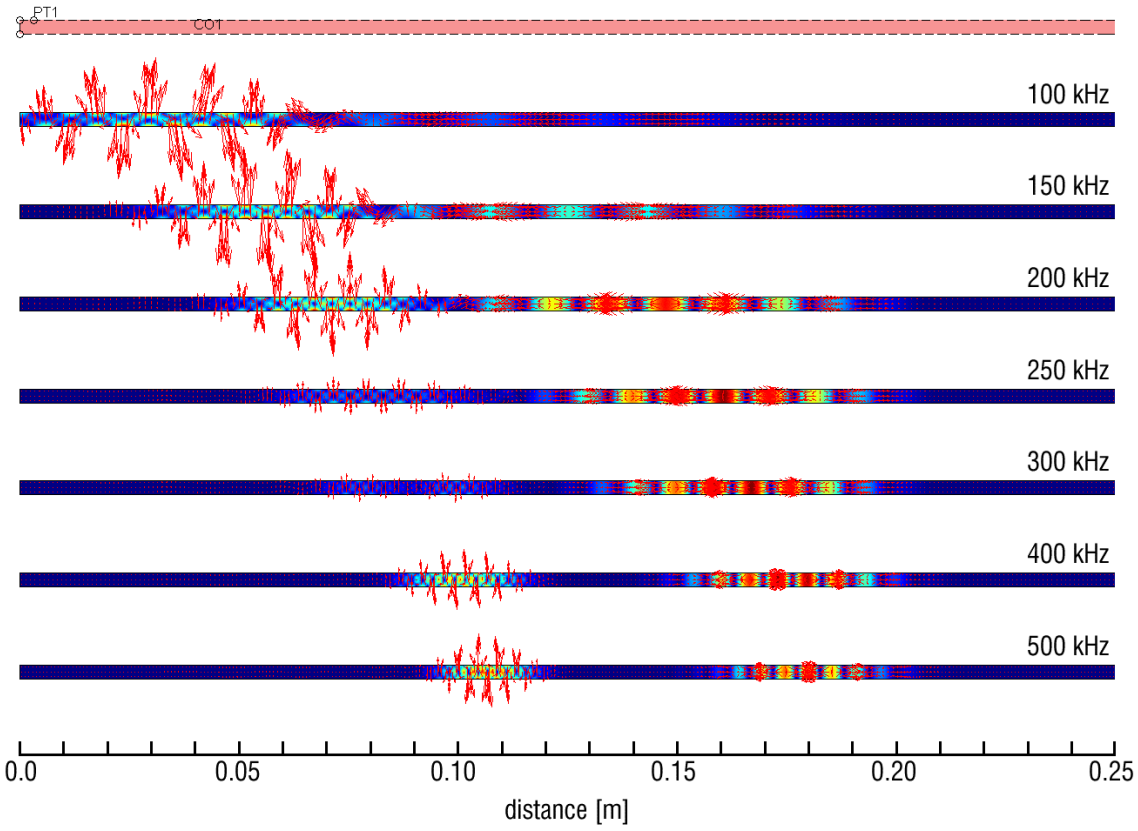

Fig. 3. Emission of A0 and S0 waves using a point-force source ($t = 40$ μs). The propagation velocity of the A0 mode increases with frequency and the emitted intensity reaches a minimum near 300 kHz. For improved visibility the plate thickness has be exaggerated by a factor of two.

To quantify the variation in the wave magnitudes with frequency, we have determined the maximum value of the x component of velocity v_x for the S0 mode and the maximum value of v_y for the A0 mode (calculated from the maximum particle velocity). These are plotted in Fig. 4 as a function of frequency (solid lines). We see a minimum in the A0 mode amplitude at approximately 283 kHz as expected and peaks in the A0 and S0 modes near the expected values of 86 kHz and 419 kHz respectively.

The point-force excitation represents a highly idealized model. In the following we will present simulations of a PZT emitting element bonded to the aluminum plate.

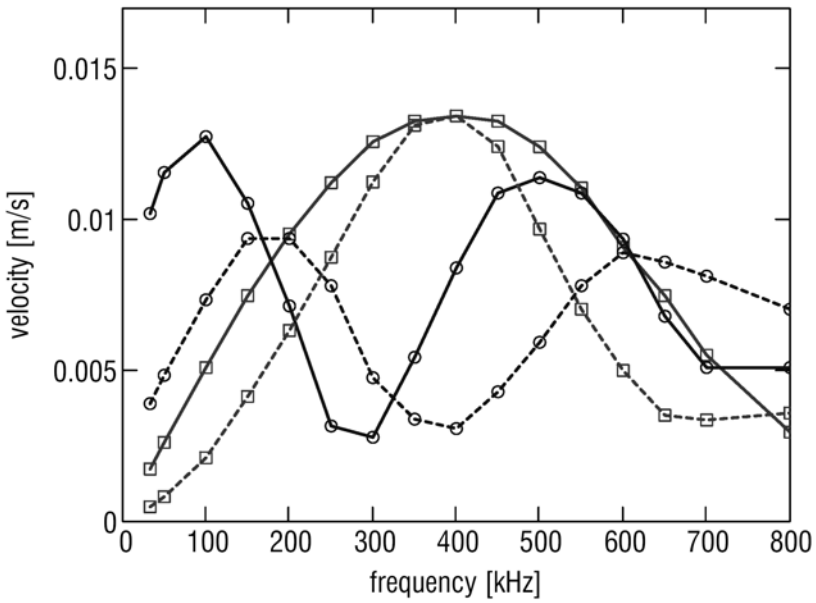

Fig. 4. Maximum particle velocity of generated waves as a function of frequency for A0 and S0 modes, obtained with the point-force model (solid lines) and with the PZT model (dashed lines). The PZT data correspond to a driving voltage of 10 volts peak-to-peak and the point force model results are scaled to match at the S0 peak.

PZT transducer as a source

We now develop a more realistic model of the wafer transducer to include details of the PZT- plate interaction. Stress, strain, electric field, and displacement in piezoelectric materials are described by a pair of coupled equations, and are conventionally expressed in matrix form representing the tensor quantities. For Motorola 3203HD PZT material, poled in the 3-direction, we express the relations between stress T, strain S, electric field E, and electric displacement D by

$$\begin{pmatrix} T_1 \\ T_2 \\ T_3 \\ T_{23} \\ T_{13} \\ T_{12} \end{pmatrix} = \begin{pmatrix} 14.2 & 9.19 & 10.2 & 0 & 0 & 0 \\ 9.19 & 14.2 & 10.2 & 0 & 0 & 0 \\ 10.2 & 10.2 & 14.1 & 0 & 0 & 0 \\ 0 & 0 & 0 & 2.55 & 0 & 0 \\ 0 & 0 & 0 & 0 & 2.55 & 0 \\ 0 & 0 & 0 & 0 & 0 & 2.51 \end{pmatrix} \begin{pmatrix} S_1 \\ S_2 \\ S_3 \\ S_{23} \\ S_{13} \\ S_{12} \end{pmatrix} \cdot 10^{10} - \begin{pmatrix} 0 & 0 & -11.7 \\ 0 & 0 & -11.7 \\ 0 & 0 & 19.7 \\ 0 & 14.3 & 0 \\ 14.3 & 0 & 0 \\ 0 & 0 & 0 \end{pmatrix} \begin{pmatrix} E_1 \\ E_2 \\ E_3 \end{pmatrix}$$

and

$$\begin{pmatrix} D_1 \\ D_2 \\ D_3 \end{pmatrix} = \begin{pmatrix} 0 & 0 & 0 & 0 & 14.3 & 0 \\ 0 & 0 & 0 & 14.3 & 0 & 0 \\ -11.7 & -11.7 & 19.7 & 0 & 0 & 0 \end{pmatrix} \begin{pmatrix} S_1 \\ S_2 \\ S_3 \\ S_{23} \\ S_{13} \\ S_{12} \end{pmatrix} + \begin{pmatrix} 1514 & 0 & 0 \\ 0 & 1514 & 0 \\ 0 & 0 & 1299 \end{pmatrix} \varepsilon_0 \begin{pmatrix} E_1 \\ E_2 \\ E_3 \end{pmatrix}$$

where stress has units of Pa, electric field has units of V/m, electric displacement has units of C/m^2, and ε_0 is the dielectric permittivity of free space. We extracted material properties from measurements reported in reference [10].

The equations above are written in the conventional form for piezoelectricity, poled in the 3-direction, whereas the two-dimensional (plane strain) geometry of the simulated system is shown in Fig. 1b. We must adapt the equations so that the 1-direction corresponds to the x-axis, and the 3-direction corresponds to the y-axis. Additionally, to impose the plane strain condition we require that strains S_2, S_{23}, and S_{12} equal zero and we apply an electric field E_y to the wafer electrodes (along the poling direction) and set E_1 and E_2 to zero. Under the conditions these conditions, the first equation reduces to

$$\begin{pmatrix} T_x \\ T_y \\ T_{xy} \end{pmatrix} = \begin{pmatrix} 14.2 & 10.2 & 0 \\ 10.2 & 14.1 & 0 \\ 0 & 0 & 2.55 \end{pmatrix} \begin{pmatrix} S_x \\ S_y \\ S_{xy} \end{pmatrix} \cdot 10^{10} - \begin{pmatrix} -11.7E_y \\ 19.7E_y \\ 0 \end{pmatrix}.$$

For the most accurate results, we should perform a multiphysics simulation coupling the electrostatic solution with the structural mechanics solution, but multiphysics simulation is computationally burdensome. Instead, for wave generation, we chose a simplified approach where we approximately model the effect of the applied electric field by appropriate external forces applied to the PZT surfaces. To see how this can be done, consider first a PZT wafer not bonded to a plate. If an electric field is applied in the *y* direction, we have

$$0 = 14.2 \cdot 10^{10} \cdot S_x + 10.2 \cdot 10^{10} \cdot S_y - (-11.7) \cdot E_y$$
$$0 = 10.2 \cdot 10^{10} \cdot S_x + 14.1 \cdot 10^{10} \cdot S_y - 19.7 \cdot E_y$$

The strain will be the same as if external forces per unit area of $11.7 \cdot E_y$ are applied to act in compression on the right and left faces while external forces per unit area of $19.7 \cdot E_y$ are applied to act in tension on the top and bottom faces. We will assume that is approximately correct to use the same external forces when the PZT wafer is bonded to a plate, as shown in Fig. 5. (As in Fig. 1b, the forces are line loads, per unit length, in the *z*-direction.) We also assume perfect bonding between the PZT wafer and the plate. This model (referred to later as the PZT force model) results in considerably reduced simulation time and improved convergence, especially when no material damping is used.

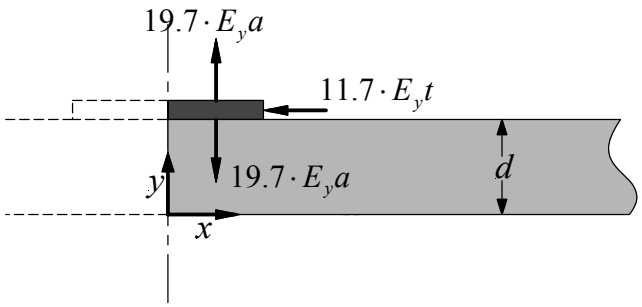

Fig. 5. Wafer transducer showing forces exerted on the surfaces to model the effect of an electric field E_y.

In order to confirm that this model is a good approximation to the real situation, we have also performed full multiphysics simulations at selected frequencies. These simulations were performed using FEMLAB 3.0 as discussed later. Figure 6 compares the full multiphysics simulations with the point force model and the PZT force model. In this figure the results from the point force model have been scaled to provide the same maximum displacement as the other models. We see that the agreement between the PZT force model and the full multiphysics calculation is excellent, both in the magnitude and detailed shape of the waves. There are significant differences between the point force model and the other two models even when the data are scaled to make the amplitude of the S0 waves the same.

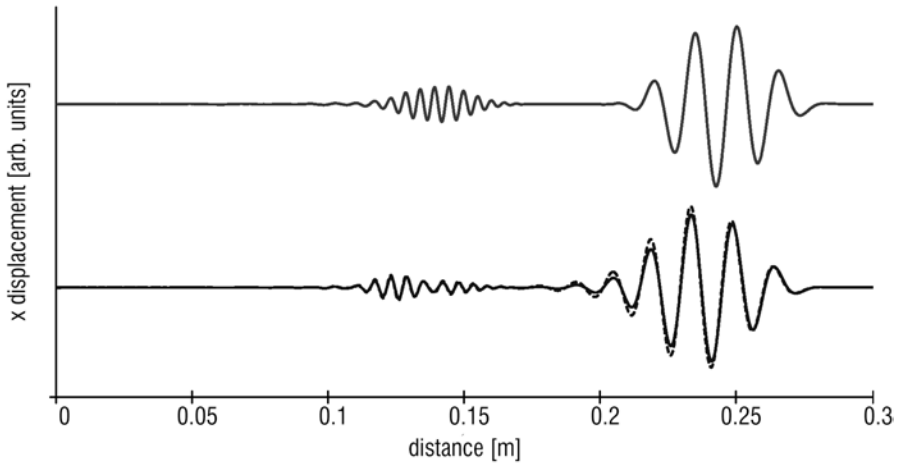

Fig. 6. Simulated x displacement for 350 kHz, t = 53 μs for three models: (top) point force model and (bottom, solid line) PZT force model and (bottom, dashed line) full multiphysics simulation. The results from the point force model are significantly different from the other two models.

Figure 7 shows complex motions in the vicinity of the PZT wafer when the PZT force model is used. The isolated PZT undergoes expansion primarily in the x direction with a much smaller contraction in the y direction. At t = 5.71 μs (corresponding to zero electric

field) there is little stress in the PZT and as a result of the previous cycle the displacements in the aluminum are in the $-x$, $-y$ directions. At $t = 6.43$ μs (corresponding to a positive peak in the applied electric field) the PZT is under high compression in the y direction and expands in the x direction, resulting in a displacement of the surface of the aluminum in the same direction. Extending the aluminum in the x direction results in a contraction in the y direction by the Poisson effect. Consequently between $t = 6.43$ μs and $t = 7.14$ μs the displacement in the x direction becomes smaller, eventually reversing sign at $t = 7.14$ μs. The following plots show the remaining half cycle. It is apparent that there are significant displacements in both the x and y directions. The y displacement in particular is more pronounced than predicted by the point-force model (not shown).

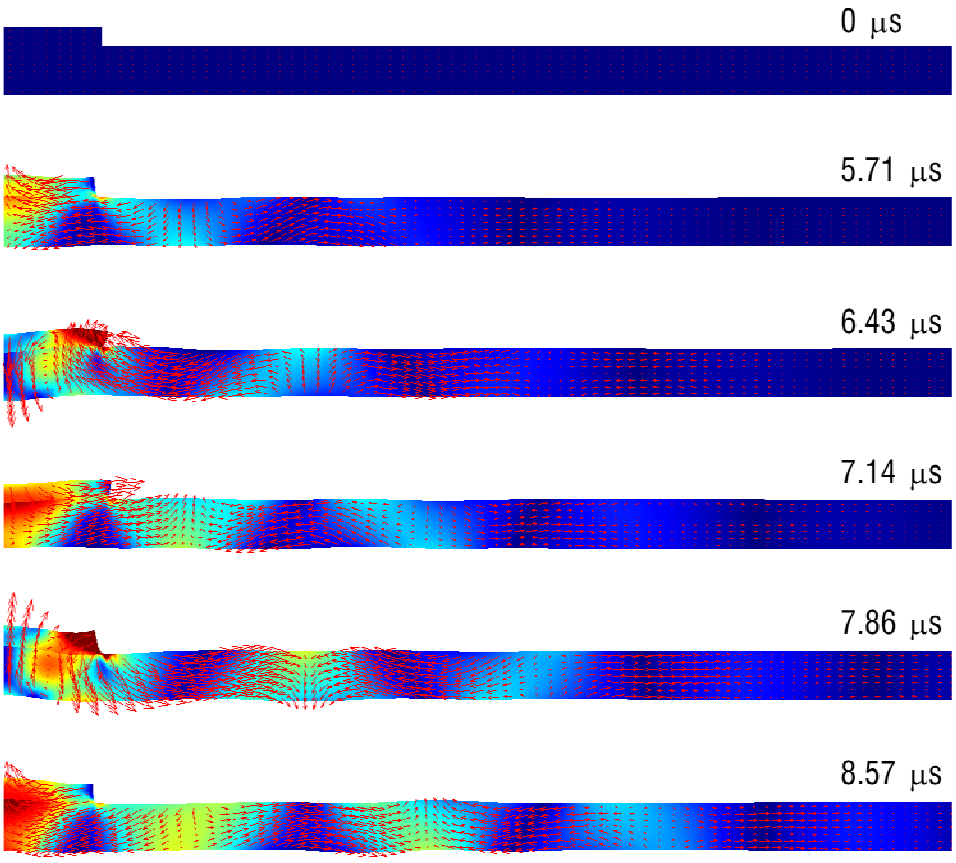

Fig. 7. Motion in the vicinity of the PZT wafer for excitation at 350 kHz (additional details in text). The outline indicates the distorted shape of the PZT and plate (greatly exaggerated for visibility). The color indicates the von Mises stress and arrows indicate the vector displacement.

Figure 8 shows the results of simulations with the PZT force model which show the propagation and separation of the wave modes with increasing time. In this diagram the thickness of the aluminum plate has been exaggerated by a factor of 3 so that the waves can be clearly seen. The A0 and S0 modes exhibit the expected behavior, including

propagation velocities which are in good agreement with the group velocities calculated from Fig. 1 (2.55×10^5 and 5.37×10^5 cm/sec for the A0 and S0 modes, respectively).

From PZT force model simulations over a range of frequency we can extract the amplitudes of the emitted waves. These results are also shown in Fig. 4. For comparison purposes the results of the point force model simulation results have been normalized to the same velocity at the S0 mode peak. The results of the PZT force model simulation are qualitatively similar but not identical to the point-force results. Qualitatively the important differences are (1) a shift of the peaks and minima to somewhat higher frequencies and (2) relatively stronger emission of waves at high frequencies than observed with point-force excitation. We continue to observe an optimum frequency at which the S0 mode is predominantly emitted.

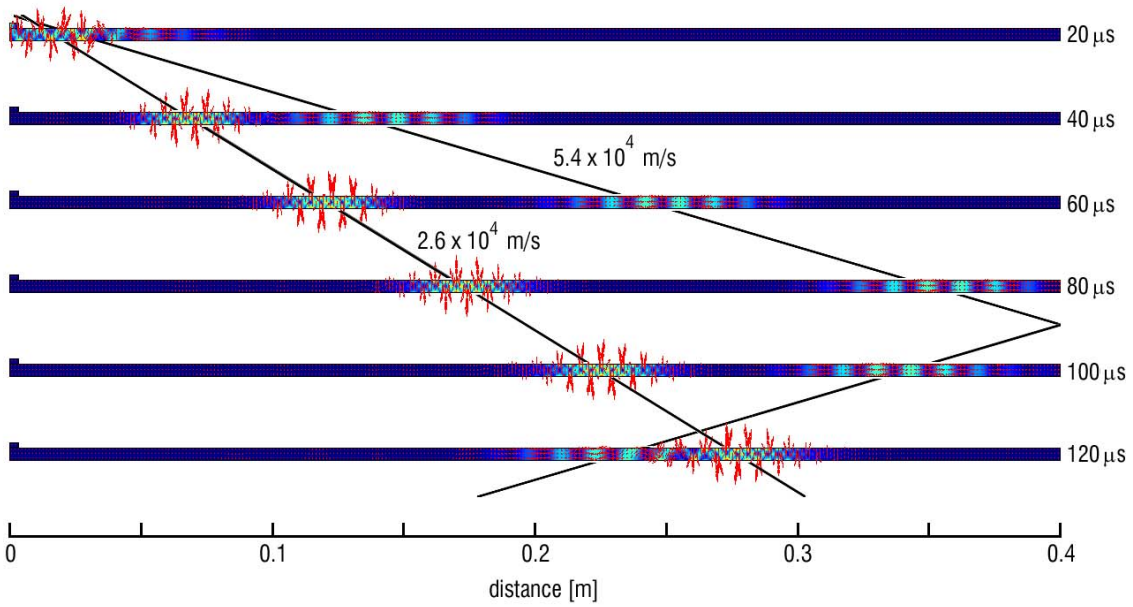

Figure 8. Propagation of A0 and S0 modes at 200 kHz. The thickness of the plate has been exaggerated by a factor of 3 for improved visibility. Color is proportional to the von Mises stress and the arrows indicate the *x* and *y* particle displacement.

III. Detection of Lamb waves

We will now consider the detection of Lamb waves. As this is the inverse process of wave generation, it may appear at first sight that the wave generation and wave detection curves should be the same. However, this is not the case. During emission the motion of the plate and PZT are symmetric about the *y* axis and undergo complex motions which later resolve into S0 and A0 modes. During detection the transducer interacts with a single mode which is propagating unidirectionally. Consequently the displacements of the PZT will not be the same as during emission.

In order to analyze the detection of Lamb waves we used a full electro-mechanical (multiphysics) simulation. These simulations were performed using the multiphysics (electrostatics plus plane-strain structural mechanics) time-dependent mode of FEMLAB

3.0 (Direct (UMFPACK) linear solver in the weak mode). The response of a receiving PZT 6.4 mm long and 0.64 mm thick was calculated separately for S0 and A0 modes. A particular mode was selectively generated by two point forces on the top and bottom of the aluminum plate. When these two sources are driven in phase (out of phase), the S0 (A0) mode is selectively launched. The bottom surface of the PZT was electrically grounded ($V = 0$) and an equipotential boundary condition was set on the top surface. The simulation yields the time-dependent mechanical displacements and also the time-dependent potential of the PZT top surface. The sensitivity for each mode was calculated by dividing the maximum top surface potential by the particle velocity for each wave.

Figure 9 shows the measured sensitivities as a function of frequency. At low frequencies the sensitivity of the PZT to the S0 mode is practically constant. In this frequency range the half-wavelength of the acoustic wave is longer than the PZT and the PZT functions as an ideal strain sensor. At higher frequencies the PZT is more than a wavelength long and the strain reverses sign along the transducer, leading to a decrease in sensitivity. The behavior of the A0 sensitivity is much different. This is because strain is related to particle velocity through the expression

$$S = \frac{du}{dx} = \frac{du}{dt}\frac{1}{c_p}$$

where S is the strain, u is the particle displacement, and c_p is the phase velocity. The phase velocity of the A0 mode is strongly frequency-dependent and decreases toward zero at low frequencies. Consequently the A0 sensitivity increases strongly with decreasing frequency. We do see evidence for the expected minimum in sensitivity near 400 kHz where the transducer is exactly one wavelength long and a maximum near 600 kHz where it is exactly 1.5 wavelengths long.

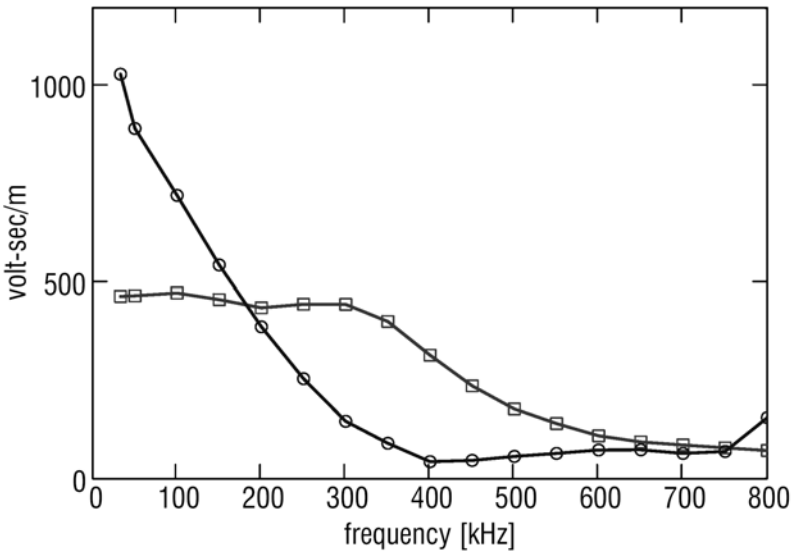

Figure 9. Simulated receiver sensitivity as a function of frequency: (circles) A0 mode and (squares) S0 mode.

In order to obtain the received signal amplitude for a given input pulse it is necessary to multiply the particle velocity per volt (from Fig. 4) with the receive sensitivity in volts per unit particle velocity (Fig. 9). This is the overall system transfer function v_{out}/v_{in} [volts/volt] and is shown in Fig. 10 as a function of the pulse center frequency. Overall the S0 and A0 peak locations are near to the predictions of eq. (1) and (2) with the S0 peak lower in frequency and the A0 peak somewhat higher. For this geometry generation of the S0 is predicted to be strongly dominant near 325 kHz.

Also shown in Fig. 10 is the predicted v_{out}/v_{in} when both transmitter and receiver are simulated using a full multiphysics calculation. These calculations are substantially more time-consuming, particularly at the extremes of high and low frequencies and onsequently we have performed these simulations only at a few selected frequencies. The results are in very good agreement with those obtained by simulating the receiver and transmitter separately. This further supports the accuracy of the PZT force model for more efficient simulation of wave emission.

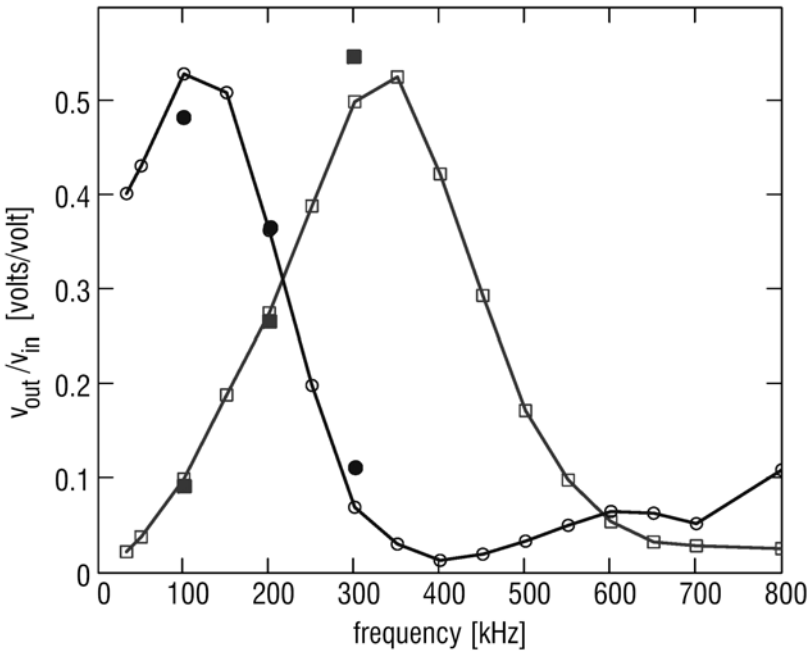

Fig. 10. Overall system transfer function v_{out}/v_{in} as a function of pulse center frequency: (■,□) S0 mode and (○,●) A0 mode. The solid points are the results from the full multiphysics simulation.

IV. Comparison with experiment

Measurements of the A0 and S0 wave amplitudes have been performed for comparison with the simulations. These measurements used an aluminum plate 0.159 cm in thickness and two PZT transducers (Motorola 3203) 0.64 cm × 1.92 cm × 0.064 cm in size. The transducers were mounted using silver epoxy (Epotek E4110-LV) approximately 20 cm apart with the long sides parallel. The transducers were far from any edges of the aluminum plate (> 50 cm) so that pulses from edge reflections were delayed by a

sufficiently long time to avoid interference with the first received A0 pulse. Data was taken by driving one transducer with a National Instruments PCI-5411 board programmed to produce the windowed sinusoidal pulse with 10 V peak amplitude. The receiving transducer was connected to a National Instruments PCI-5112 100 MHz bandwidth analog input board and 5000-10000 samples were collected using Labview. Some typical data are shown in Fig. 11. The first pulse arrival is the S0 mode and as expected the amplitude of this mode reaches a maximum near 350 kHz. The A0 mode pulse arrives later with a minimum near 400 kHz.

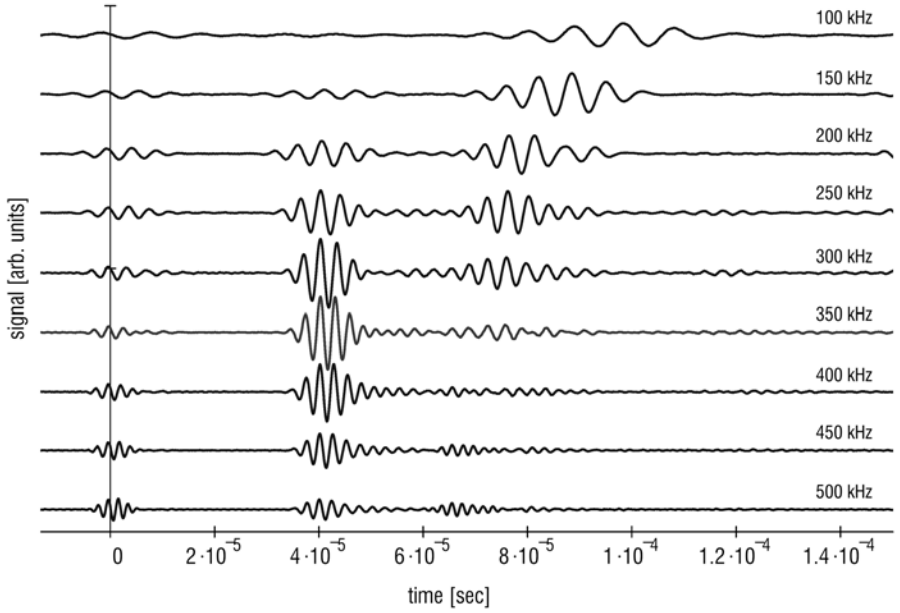

Fig. 11. Received signals as a function of frequency (20 cm separation). The arrow marks the center of the transmitter pulse train.

Figure 12 plots the ratio of the exciting pulse amplitude to the maximum received pulse amplitude as a function of frequency. Results are shown for three different transducer pairs, all separated by 20 cm. The results obtained for different transducer pairs are quite similar for the S0 mode in both amplitude and frequency dependence, while the A0 results are significantly different.

For the S0 mode, we observe good agreement between experiment and theory with respect to the peak position and the frequency dependence. Experimentally the peak S0 response is at 300-325 kHz kHz compared to the simulated peak at 350 kHz. Note that eq. (2) predicted a peak S0 response at 419 kHz, which is close to but somewhat higher than the experimental results.

The agreement between experiment and simulations for the A0 mode is poor, with the simulations predicting a higher peak amplitude than actually observed and also a peak at a substantially lower frequency. Note that the simulated peak position is approximately at 100 kHz, which is in good agreement with eq. (3) and also in good agreement with the measurements reported by Giurgiutiu [9] for a transducer of almost the same length (0.7 cm compared to 0.64 cm in our experiments.)

We have ruled out instrumental artifacts as an explanation for the discrepancy between simulations and experiment. Measurements with several different transducer pairs consistently show the same S0 peak position and also approximately the same S0 amplitude. The A0 data exhibits significant variability between transducer pairs.

We are attributing the poor agreement between the A0 experiment and simulation to nonideal bonding between the PZT wafer and the aluminum sheet. This is supported by our observations of some differences in the measured impedance spectrum for different transducers which are consistent with imperfect bonding (not shown). Apparently the A0 mode is more sensitive to the bonding conditions than the S0 mode. It is important to note that the published measurements by Giurgiutiu [9] show that with appropriate bonding conditions results in better agreement with simulations can be obtained. Also note that the S0 mode may be preferable in applications as it can be generated selectively and also because it exhibits little dispersion over a wide frequency range.

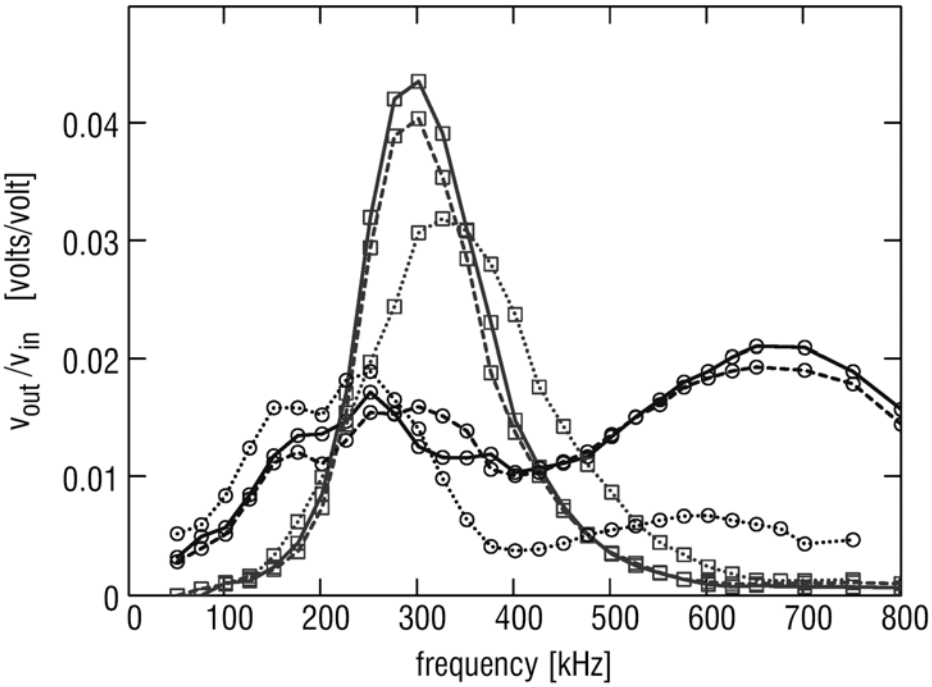

Figure 12. Measurements of the ratio of the peak output signal to the peak of the exciting pulse for three transducer pairs.

V. Transducer design guidelines

We will now determine the optimum PZT thickness for the case in which the exciting voltage is fixed. We first discuss qualitatively the effect of varying the PZT thickness. If the PZT is very thick, the strain in the aluminum beneath the PZT should be roughly equal to that in an unbonded PZT. Since the strain in an unbonded PZT is proportional to the applied electric field, we expect

$$S_x \propto E_z = \frac{V}{t}$$

and as a result the emitted S0 wave amplitude increases with decreasing thickness. As the PZT becomes thinner, the field-induced strain is shared between the aluminum and the PZT. For very thin PZT there is essentially no strain in the PZT. Consequently, we expect an optimum at an intermediate thickness. Figure 13a shows the emitted velocities as a function of PZT thickness at 350 kHz. This optimum occurs for a PZT thickness less that the aluminum thickness because the stiffness of the PZT at constant electric field is approximately a factor of three greater than the aluminum stiffness. Figure 13b shows a similar calculation for the dependence of receive sensitivity on PZT thickness at 350 kHz. Again there is an optimum PZT thickness near 0.5 mm. These results show that near-optimum overall performance can be obtained by using the same PZT transducer for transmit and receive.

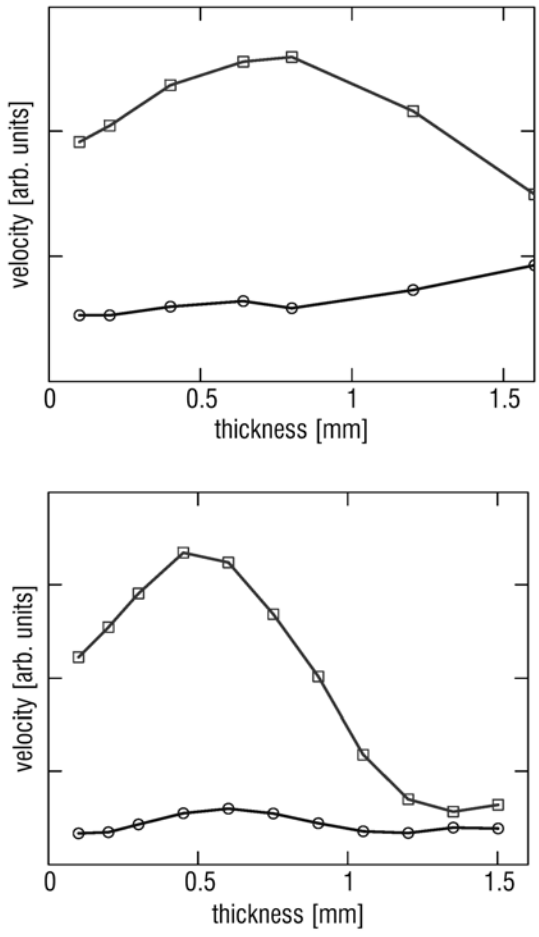

Figure 13. Effect of transducer thickness: (top) emitted A0 (circles) and S0 (squares) wave amplitudes as a function of PZT thickness at 350 kHz; (bottom) A0 (circles) and S0 (squares) receive sensitivity as a function of PZT thickness at 350 kHz.

These results can be used to draw some general conclusions about the preferred transducer dimensions and operating frequency. We assume that pulse dispersion is undesirable and that selective generation of a single mode is preferred. Selective generation of the S0 with respect to the A0 mode is easily achieved in the low-frequency region where the S0 and A0 phase velocities are appreciably different. We have seen that equations (1) and (2) derived from the point-force model provide a rough estimate of the frequencies of maximum and minimum response. In general one should choose the transducer length and center frequency so that the S0 mode is near its peak frequency and the A0 mode near its minimum. To first order, one should locate the $f \cdot d$ product corresponding to $v_{phase}(\mathrm{S0}) = 2 \cdot v_{phase}(\mathrm{A0})$. For a given plate thickness d this determines the center frequency f. Then the transducer length is determined from $a = v_{phase}(\mathrm{S0})/4f$.

While this approach can be used for initial calculations, finite element simulations will yield more precise values for the peak and minimum frequencies and the mode selectivity. In addition, finite element simulations make it possible to determine the optimum transducer thickness, which cannot be calculated using the point-force model. While the optimum transducer thickness is different for emission and reception, for the case examined here the optimum occurs nearly at the same thickness.

VI. Conclusions

In this paper, the operation of a PZT wafer transducer was analyzed for the generation and detection of guided acoustic waves using a combination of finite element simulation and experiments. The simulations account for the detailed mechanical interactions between the transducer and the transmitting medium, and in addition include a full multiphysics representation of the pulse reception.

The simulations and the experimental results demonstrate that a piezoelectric wafer transducer can be used for selective excitation of the S0 mode. The point-force model has proven to be a useful tool to analyze the qualitative behavior of the transducer. A more advanced PZT force model and a full piezo finite element model were introduced that are a closer representation of the real system. For the wave generation there is very little difference between the PZT force model and the full piezo model. For the wave detection only the piezo model can be used. A comparison of finite element simulations with experimental results showed that the more advanced models show a better match and demonstrated these models can be used for a quantitative analysis of the piezo wafer transducer.

Acknowledgements

The authors wish to acknowledge support from the Bosch Research and Technology Center North America, Pittsburgh, PA, USA and from the National Science Foundation under grant CMS-0329880. Any opinions, findings, and conclusions or recommendations expressed in this material are those of the authors and do not necessarily reflect the views of the National Science Foundation.

References

[1] J.L. Rose, "Guided Wave Nuances for Ultrasonic Nondestructive Evaluation," IEEE Trans. Ultrasonics, Ferroelectrics, and Frequency Control, vol. 47, 575-583 (May, 2000)

[2] M.J. Quarry and J.L. Rose, "Multimode guided wave inspection of piping using comb transducers," Mater. Eval. 57, 1089-1090 (1999).

[3] J.L. Rose, S. Pelts, and M. Quarry, "A comb transducer model for guided wave NDE," Ultrasonics 36, 163-168 (1998).

[4] W. Zhu and R.L. Rose, "Lamb wave generation and reception with time-delay periodic linear arrays: A BEM simulation and experimental study," IEEE Trans. Ultrasonics, Ferroelectrics, and Frequency Control 46, 654-664 (1999).

[5] J. Li and J.L. Rose, "Implementing guided wave mode control by use of a phased transducer array," IEEE Trans. Ultrasonics, Ferroelectrics, and Frequency Control 48, 761-768 (2001).

[6] Kessler S.S., Spearing S.M., Atalla M.J., Cesnik C.E.S. and C. Soutis. "Damage Detection in Composite Materials using Frequency Response Methods." Proceedings of the SPIE's 8th International Symposium on Smart Structures and Materials, 4-8 March 2001, Newport Beach, CA.

[7] V. Giurgiutiu and A.N. Zagrai, "Characterization of piezoelectric wafer active sensors," Journal of Intelligent Material Systems and Structures 11, 959-975 (2000).

[8] Kessler S.S., Spearing S.M. and C. Soutis. "Structural Health Monitoring of Built-up Composite Structures using Lamb Wave Methods." Submitted for publication to Journal of Intelligent Material Systems and Structures.

[9] V. Giurgiutiu, "Lamb Wave Generation with Piezoelectric Wafer Active Sensors for Structural Health Monitoring," Smart Structures and Materials 2003: Smart Structures and Integrated Systems, 111

[10] S. Sherrit, H. D. Wiederick, B. K. Mukherjee, "A complete characterization of the piezoelectric, dielectric, and elastic properties of Motorola PZT 3203 HD including losses and dispersion," *Proc. SPIE Medical Imaging Conf.*, SPIE 3037, 158-169 (1997).